



HAL
open science

Diffusive transport of gases in saturated nanopores: Caprock leakage from a molecular simulation perspective

Brahim Benazzouz, Khac Hieu Ho, Phuoc The Nguyen, Hai Hoang, Guillaume Galliero

► To cite this version:

Brahim Benazzouz, Khac Hieu Ho, Phuoc The Nguyen, Hai Hoang, Guillaume Galliero. Diffusive transport of gases in saturated nanopores: Caprock leakage from a molecular simulation perspective. Journal of Natural Gas Science and Engineering, 2022, 98, pp.104383. 10.1016/j.jngse.2021.104383 . hal-03962180

HAL Id: hal-03962180

<https://univ-pau.hal.science/hal-03962180>

Submitted on 8 Jan 2024

HAL is a multi-disciplinary open access archive for the deposit and dissemination of scientific research documents, whether they are published or not. The documents may come from teaching and research institutions in France or abroad, or from public or private research centers.

L'archive ouverte pluridisciplinaire **HAL**, est destinée au dépôt et à la diffusion de documents scientifiques de niveau recherche, publiés ou non, émanant des établissements d'enseignement et de recherche français ou étrangers, des laboratoires publics ou privés.



Distributed under a Creative Commons Attribution - NonCommercial 4.0 International License

Diffusive Transport of Gases in Saturated Nanopores: Caprock Leakage from a Molecular Simulation Perspective

Brahim K. Benazzouz¹, Khac Hieu Ho^{2,3}, Phuoc The Nguyen^{2,3}, Hai Hoang^{3,4}, Guillaume Galliero^{4*}

¹Department of Civil Engineering, National Polytechnic School (ENP), 10 Avenue Hassen Badi El Harrach BP 182, 16200, Algiers, Algeria

²Institute of Research and Development, Duy Tan University, Da Nang 550000, Viet Nam.

³Faculty of Environmental and Natural Sciences, Duy Tan University, 03 Quang Trung Street, Da Nang, Vietnam

⁴Laboratoire des Fluides Complexes et leurs Réservoirs, LFCR, UMR 5150, Université de Pau et des Pays de l'Adour, E2S UPPA, CNRS, TotalEnergies, 64000, Pau, France

Corresponding Author: *guillaume.galliero@univ-pau.fr

Abstract

In this work, molecular dynamics simulations have been performed to shed some light on possible gas leakages by molecular diffusion through reservoir caprocks. To do so, solubility and transport diffusivity of light hydrocarbon gases (methane and ethane) in water-saturated slit nanopores have been investigated at typical reservoir thermodynamics conditions. Interestingly, it has been noticed that the gas solubility in the saturated nanopores is noticeably higher than in the bulk state. This “oversolubility” is mainly due to an adsorption-driven effect for both gases. However, a non-negligible confinement-driven effect has also been noticed for ethane. As a consequence, the oversolubility linearly increases with the reciprocal of the pore size. Regarding the transport diffusivity, results have shown that it decreases with the decrease of the pore size. However, rather surprisingly, from the transport diffusivity point of view, the pore size has a weaker impact on ethane than on methane. This is probably related to the fact that ethane is preferentially localized at the depleted water region in the nanopore, whereas methane is mainly localized at the adsorbed water region. Finally, these results have been used to estimate the influence of these nano-confinement effects on the diffusive gases leakages through a modelled water-saturated caprock over geological times. It has been found that the estimated leakage could be noticeably enhanced by the nano-confinement effects, emphasizing the importance of taking into account these effects on gas leakage estimates through caprock.

Keywords: Oversolubility, Molecular Diffusion, Nanopores, Gases, Molecular Simulations

1. Introduction

Caprock is often viewed as an impermeable rock type trapping fluids in reservoirs as discussed in (Grunau, 1987; Krooss et al., 1988; Schlömer and Krooss, 1997; Selley and Sonnenberg, 2015). When considering the gas trapping, the sealing efficiency of caprock arises from the very tight nature of the porous medium, composed mostly of nanopores saturated by water in which most gases hardly solubilize. However, recent studies have shown that the solubility of gases in water confined in nanoporous materials, such as clay, can be noticeably greater than that in bulk water (Sun and Duan, 2007; Phan et al., 2014; Yuan et al., 2014; Ho et al., 2015; Li et al., 2016; Liu et al., 2020; Grekov et al., 2020). This “oversolubility” phenomenon, combined with molecular diffusion process, may induce a more important than scheduled leakage of gases (hydrocarbons, carbon dioxide...) through a reservoir caprock, when considering typical geological timescales, i.e. from thousands to millions of years which are the typical timescales occurring in geological engineering and in petroleum system (Krooss et al., 1988; Krooss et al., 1992a; Krooss et al., 1992b; Krooss, 1992; Schlömer and Krooss, 1997; Song and Zhang, 2013). Furthermore, considering the reservoir as an open system, i.e. subject to a gas leakage through the caprock, has a strong impact on the way the vertical fluid distribution should be modeled at the initial state in a reservoir as shown in (Montel et al., 2007). Thus, to improve the pre-evaluation of hydrocarbon amounts and distribution in the reservoirs using up to date models (Montel et al., 2007; Dembicki, 2016; Baghooee et al., 2021), or to better understand and determine sources and origins of groundwater contamination (Nowamooz et al., 2015), this overlooked possible leakage phenomenon may worth of investigations which is the purpose of this work.

Solubility and molecular diffusion of hydrocarbons gases in water-saturated nanopores, that are required to estimate the diffusion leakages through the caprock (Krooss et al., 1992a; Krooss et al., 1992b; Schlömer and Krooss, 1997), have attracted interest and attention over the years (Sun and Duan, 2007; Campos et al., 2009; Phan et al., 2014; Yuan et al., 2014; Ho et al., 2015; Li et al., 2016; Phan et al., 2016; Bui et al., 2017; Gadikota et al., 2017; Grekov et al., 2020; Liu et al., 2020). Many works, including simulations and experiments, have found that these quantities can be significantly different from those in bulk liquid water. More precisely, in nanoporous structure the solubility of various gases in the confined water can be largely enhanced compared to what occurs in bulk water (Sun and Duan, 2007; Campos et al., 2009; Ho et al., 2015), a phenomenon sometimes called “oversolubility”, and the gas molecular diffusion can be highly reduced (Phan et al., 2016; Bui et al., 2017; Gadikota et al., 2017). These phenomena are attributed to direct and indirect

effects (Phan et al., 2014; Ho et al., 2015; Li et al., 2016; Phan et al., 2016; Bui et al., 2017). The direct effect results from the gas-wall interaction, which can lead to an adsorption of gases on the pore walls (Ho et al., 2015; Li et al., 2016). The indirect effect emerges from the spatial variation of local properties of the confined liquid water due to the water-solid surface interaction, which can have a noticeable impact on the solubility and molecular diffusion of the gases (Phan et al., 2014; Phan et al., 2016; Bui et al., 2017). In nanopores, where the surface-to-volume ratio is very high, these effects may be significant (Karniadakis et al., 2004; Israelachvili, 2010). Thus, when considering nanopores, the pore size is among the major factors that influences both solubility and mass diffusion of gases (Sun and Duan, 2007; Campos et al., 2009). The systematic evaluation of such an effect on idealized systems is the main goal of the present work.

Molecular dynamics (MD) simulation has shown to be an efficient numerical tool to investigate thermodynamic and transport properties of nanoscale systems and to deal with extreme thermodynamic conditions, e.g. high pressures as found in reservoirs (Allen and Tildesley, 1987; Smit and Frenkel, 2002; Hoang et al., 2017; 2019; 2021). This tool has been used to investigate either the solubility or the molecular diffusion of various gases in solvents confined in nanopores, often at ambient conditions (Campos et al., 2009; Phan et al., 2014; Phan et al., 2016; Bui et al., 2017; Gadikota et al., 2017), yielding results consistent with experiments (Phan et al., 2014; Gadikota et al., 2017). Interestingly, this numerical tool can provide many information at the molecular scale, such as thermophysical and transport properties (Allen and Tildesley, 1987; Smit and Frenkel, 2002;), so facilitating the interpretation of the results (Phan et al., 2014; Phan et al., 2016; Bui et al., 2017). Thus, in this work, MD simulation has been employed to investigate the effect of pore size on both solubilities and molecular diffusion of light hydrocarbons gases, methane and ethane, in water-saturated nano-pores, i.e. pore sizes typical of that encountered in a caprock, at typical reservoir conditions.

This article is organized as follows. In section 2, some details on the MD simulations are described. Then, results obtained from the molecular dynamics simulations are presented and discussed in section 3. Finally, the conclusion that summarizes the main outcomes is provided in section 4.

2. Models and Simulation

2.1. Fluid and solid models

For the sake of simplicity, and because caprock complexity in terms of porous structure and fluid composition is not accessible to molecular simulations, all hydrocarbon gases (methane and ethane), water and solid molecules have been modelled using one of the simplest coarse-grained models, the Lennard-Jones one. Thus, all interactions between particles have been described by a classical Lennard-Jones (LJ) potential (Lennard-Jones, 1937) as:

$$U_{LJ}(r) = 4\epsilon \left[\left(\frac{\sigma}{r} \right)^{12} - \left(\frac{\sigma}{r} \right)^6 \right] \quad (1)$$

where, r is the distance between the two particles, ϵ is the potential depth, σ is the particle “diameter”. This simple model has shown to simultaneously predict rather well thermodynamic and transport properties of small hydrocarbons gases, i.e. methane and ethane (Galliero et al., 2006). The LJ parameters of methane used are those coming from the study of Martin and Siepmann (Martin and Siepmann, 1998), and for ethane, they were obtained from Galliero et al. (Galliero et al., 2006). They are given in Table 1.

When considering a LJ coarse-grained representation of species exhibiting polar or hydrogen bonding interaction, the effective LJ parameters should vary with the thermodynamic state to provide a good prediction for both thermodynamic and transport properties (Müller and Gelb, 2003; Hadley and McCabe, 2012). Thus, the LJ parameters of water molecules at the two studied reservoir conditions (T=373.15 K, P=50 MPa and T=423.15 K, P=100 MPa) have been adjusted to simultaneously provide a good agreement with density and viscosity data taken from the NIST reference database (Lemmon et al., 2007). The LJ equation of equation of Kolafa and Nezbeda (Kolafa and Nezbeda, 1994), and the LJ viscosity correlation of Galliero et al. (Galliero et al., 2005) were employed to perform the adjustment of water LJ parameters. Results are listed in Table 1.

Table 1: Lennard-Jones parameters of fluid molecules.

Fluid	σ (nm)	ϵ (kJ/mol)
Water (T=373K)	0.2876	3.500
Water (T=423K)	0.2805	3.200
Methane	0.3723	1.245
Ethane	0.4239	1.978

The nanopore walls have been modelled to represent the macroscopic characteristics of typical silicate mineral surfaces from the surface energy point of view. They are made of identical spherical particles arranged on a faced centered cubic (FCC) lattice. The LJ diameter

of solid particles and the lattice size have been chosen to quantitatively mimic the roughness of silicate mineral surface. The LJ energy of solid particles has been selected to yield reasonable Hamaker constant of silicate mineral surface of about $H_{ss} = 1 \times 10^{-19}$ Joule (Iwamatsu, 1998). The parameters of the solid walls are shown in Table 2.

Table 2: Lennard-Jones parameters and lattice size of solid wall.

σ (nm)	ϵ (kJ/mol)	Lattice size (nm)
0.3160	0.762	0.4469

The LJ potential parameters of the interaction between unlike molecules were calculated by using modified Lorentz-Berthelot rules (Schnabel et al., 2007):

$$\epsilon_{ij} = k_{ij} \sqrt{\epsilon_i \epsilon_j} \quad (2a)$$

$$\sigma_{ij} = \frac{1}{2} (\sigma_i + \sigma_j) \quad (2b)$$

where, i and j indicate the species, and k_{ij} is a pre-factor which was introduced to modulate the strength of energy between species (Schnabel et al., 2007). Such a parameter is often used to better model cross interactions between asymmetric molecules (Hamani et al., 2020). k_{ij} have been set to 1.0 for the interactions between the fluids (hydrocarbons gases and water) and solid walls. Between the gases and the water, k_{ij} have been adjusted to provide good solubilities of gases in bulk liquid water, as detailed in section 3.1.

2.2 Simulated configuration

To determine the properties of light hydrocarbon gases in the saturated nanopores, MD simulations in the grand canonical ensemble were performed by using a scheme similar to the one proposed in (Hoang and Galliero, 2012a), as sketched in Fig 1a. In terms of thermodynamics conditions, two reservoir conditions have been considered: (1) T=373.15 K and P=50 MPa, and (2) T=423.15 K and P=100 MPa. To address the effect of pore size on solubility and molecular diffusion of gases, MD simulations have been performed on systems with various pore sizes, W , ranging from 5 to 10 times the diameter of a gas molecule, i.e. from about 1.90 nm to about 4.24 nm, as one would expect in an ideal caprock (Schlömer and Krooss, 1997; Kampman et al., 2016; Espinoza and Santamarina, 2017). Such pore sizes correspond to permeability, k , of the micro-Darcy order of magnitude (k scales with W^2) as those found in caprocks, even if defining correctly permeability in such nanopore from geometric argument only is questionable due to the strong variations of the confined fluid properties (Hoang and Galliero, 2013).

In details, the solid walls are placed in the middle of the simulation box in the direction y , and at the top and the bottom in the direction x . Each solid wall is composed of $4 \times 10 \times 10$ FCC cells in the x , y and z direction respectively. They are separated by a distance W in the x direction, defined as the distance between two innermost opposing atomic solid layers. The walls are of finite size in the x and y directions, whereas they are extended through the whole cell in the z direction. In the reservoirs that are located sufficiently away from the solid walls to avoid the effects of the finite solid wall size in the y direction (Hoang and Galliero, 2012a), the temperature and pressure of the fluids are kept constant.

The initial configuration to compute mass diffusion coefficient and solubility of gases in the nanopores were setup as follows. First, grand-canonical molecular dynamics (GCMD) simulations were performed to equilibrate separately two systems: one consisting of water and solid molecules, and one containing gases (methane/ethane) and water, as illustrated in Figs. 1a and 1b, respectively. Then, the water molecules in the pore of the first system and the fluid (gases + water) molecules in the reservoirs of the second system were brought together to set up the initial configuration, see Fig. 1. The simulation systems contain at least 1000 water molecules and 5000 gas molecules.

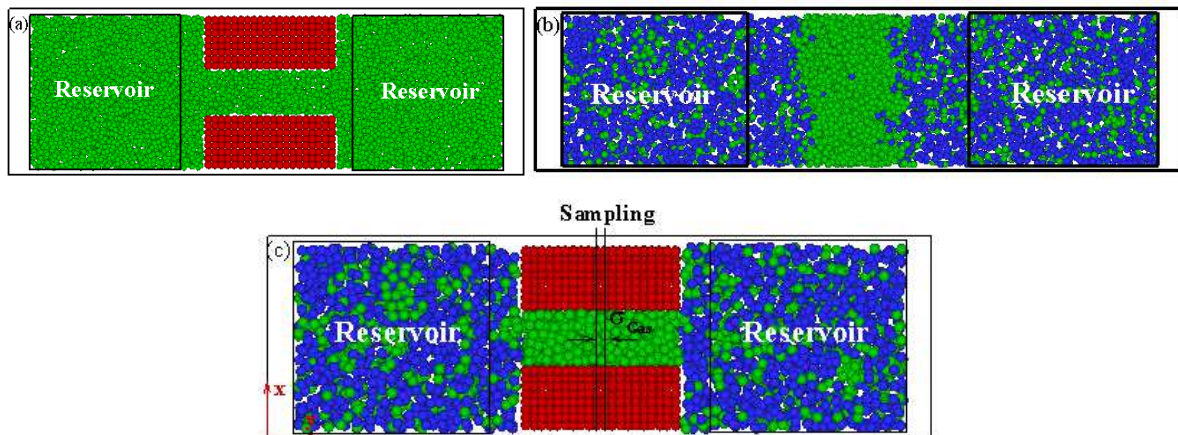


Figure 1: (a) Equilibrated system of water with the nanopore. (b) Equilibrated system containing gas and water. (c) Initial configuration of the simulated system to determine diffusion and solubility of gases in the nanopore. Red color corresponds to the solid particle, green color to water molecules and blue color to gas molecules.

2.3 Simulation details

During MD simulations, which were performed using an in-house code (Hoang and Galliero, 2012a; 2013), the equations of motion of fluid particles were integrated using the velocity-Verlet algorithm with a timestep $\delta t \approx 0.0023\text{ps}$ (Verlet, 1967), whereas the solid

particles were fixed at their sites on the FCC lattice. Periodic boundary conditions were applied in all the directions (Allen and Tildesley, 1987; Smit and Frenkel, 2002). The temperature and pressure in the reservoirs were maintained at reservoir conditions by using a Berendsen thermostat and barostat, respectively (Berendsen et al., 1984). The sampling region, of a width equal to σ_{Gas} , where the properties of the confined fluids were computed, was chosen to be located at the center of the pore in the y direction to avoid effects due to the finite size of the solid walls (Hoang and Galliero, 2012a; 2013), see Fig. 1a.

After having built the initial configuration, as detailed previously, the GCMD simulations were performed in two steps. First, the systems were equilibrated on 2×10^6 time steps, during which data in the sample region were collected to analyze the molecular diffusion of hydrocarbons gases during the unsteady regime. Then, a run of 2×10^6 time steps was achieved to compute the gas solubility and all equilibrium properties of the confined fluids.

3. Results and Discussions

3.1. Determination of the k_{ij} between gases and water

Similarly to what is done when using a Soreide and Whitson Equation of State (Soreide and Whitson, 1992), the k_{ij} of the interactions between the light hydrocarbons gases (methane/ethane) and water molecules have been selected to reproduce the experiment solubility (hereafter, the solubility is defined as a molar fraction and is noted S) of the gases in water at the studied thermodynamic reservoir conditions. More precisely, the values of k_{ij} of methane-water interaction have been adjusted to yield $S_{\text{C1,Bulk}} = 0.39\%$ and $S_{\text{C1,Bulk}} = 0.78\%$ at (T=373.15 K, P=50 MPa) and (T=423.15 K, P=100 MPa), respectively (Duan and Mao, 2006). For the ethane-water interaction, they were adjusted to provide $S_{\text{C2,Bulk}} = 0.13\%$ at (T=373.15 K, P=50 MPa) and $S_{\text{C2,Bulk}} = 0.28\%$ at (T=423.15 K, P=100 MPa) (Mao et al., 2005). For this purpose, the gas solubility dependence on k_{ij} in water has been estimated at the studied thermodynamic reservoir conditions by performing GCMD simulations on systems containing gas and water as shown in Fig. 1b. Simulation results are illustrated in Fig. 2.

The results clearly show that the gas solubility monotonously increases with k_{ij} in all cases, allowing to estimate the optimal k_{ij} by interpolating the simulation data. Optimized k_{ij} values are provided in Table 3. It is worth noticing that the k_{ij} significantly varies with the thermodynamic conditions. This can be probably understood from the strong dependence of

the LJ potential parameters of coarse-grained water molecules on the thermodynamic conditions, see Table 2. In the following, these k_{ij} values have been employed to estimate the solubility and the molecular diffusion of methane and ethane in the saturated nanopores.

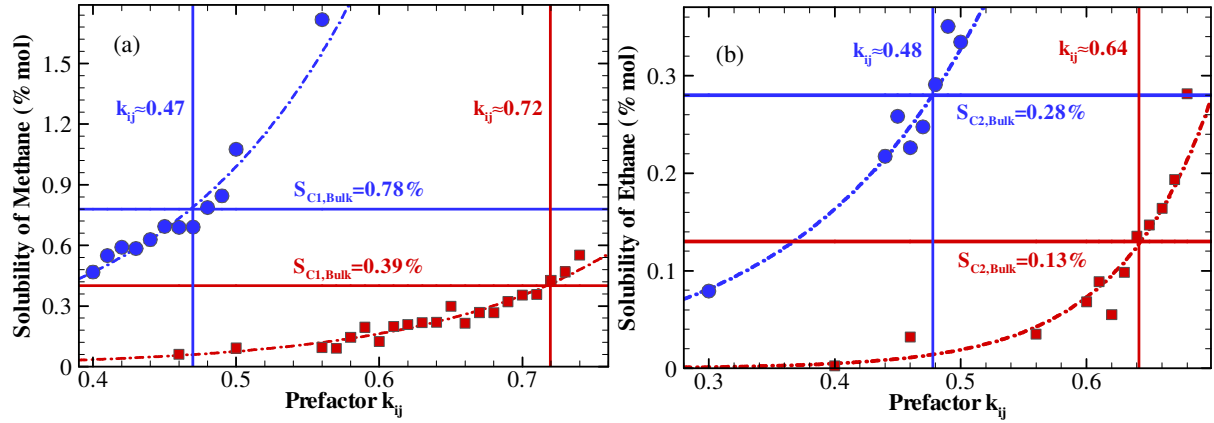


Figure 2: Dependence of hydrocarbon gas solubility in bulk liquid water on k_{ij} (a): Methane. (b): Ethane. (Red color) Squares corresponds to $T = 373.15\text{K}$ and $P = 50\text{MPa}$. (Blue color) and circles to $T = 423.15\text{K}$ and $P = 100\text{MPa}$. Dashed-Dotted curves are exponential fitting functions. Solid horizontal and vertical lines correspond to the experimental solubility of gases in water and the optimized k_{ij} values, respectively.

Table 3: Optimized k_{ij} between methane/ethane and water.

	Water ($T=373\text{K}$)	Water ($T=423\text{K}$)
Methane	0.72	0.47
Ethane	0.64	0.48

3.2. Effect of the pore size on solubility

3.2.1. Methane

Figure 3 shows the solubility of methane in the saturated nanopores for the two studied reservoir conditions and for pore sizes ranging from 1.86 nm to 3.72 nm. As expected, the solubility of methane in the nanopores is noticeably larger than that in bulk water (Campos et al., 2009, Ho et al., 2015), up to three times the bulk value for the smallest pore. To better understand this behavior, the local solubility profiles along the x direction have been computed. As shown in Fig. 4, the increase of solubility results from a local solubility which is significantly larger (up to about fifteen times) in the vicinity of the solid surfaces than in the center of the pore which exhibits solubility values similar to what found in bulk water, as expected.

Regarding the physical origins of the increase of solubility of gases in saturated nanopores, two possible molecular mechanisms have been proposed in the literature (Ho et al., 2013): (1) Adsorption-driven effect and (2) Confinement-driven effect. The adsorption-driven effect corresponds to an adsorbed gas layer at a distance of about $\sigma_{\text{solid-gas}}$ from the solid surface (Ho et al., 2013; 2015). The confinement-driven effect is related to a gas layer

localized around the solvent depleted zone (Ho et al., 2013; 2015). In our systems, results illustrated in Fig. 5 indicate that the methane peak is mostly located at a distance around $\sigma_{\text{solid-gas}}$ from the solid surface, indicating so that the adsorption-driven effect has a dominant effect on the increase of solubility of methane in the simulated systems.

To quantify the increase of solubility due to the confinement, the oversolubility, ΔS_{Gas} , has been computed. It is defined as the difference between the solubilities of gas in nanopore and in bulk water by:

$$\Delta S_{\text{Gas}} = S_{\text{Gas,Pore}} - S_{\text{Gas,Bulk}} \quad (3)$$

where $S_{\text{Gas,Pore}}$ is the solubility of gas in the nanopore and $S_{\text{Gas,Bulk}}$ the value in the bulk. Results are shown in Fig. 3. It has been found that the oversolubility increases linearly with the inverse of the pore size. This feature is consistent with experiment results (Sun and Duan, 2007; Miachon et al., 2013) and is simply due to the adsorption-driven nature of this phenomenon and because the local increase of solubility does not depend much on the confinement, see Fig. 4. In addition, the oversolubility is the largest for the highest reservoir temperature. This effect is subtle and is probably related to temperature effects that are stronger than pressure effects on water in terms of structure, see Fig. 5.

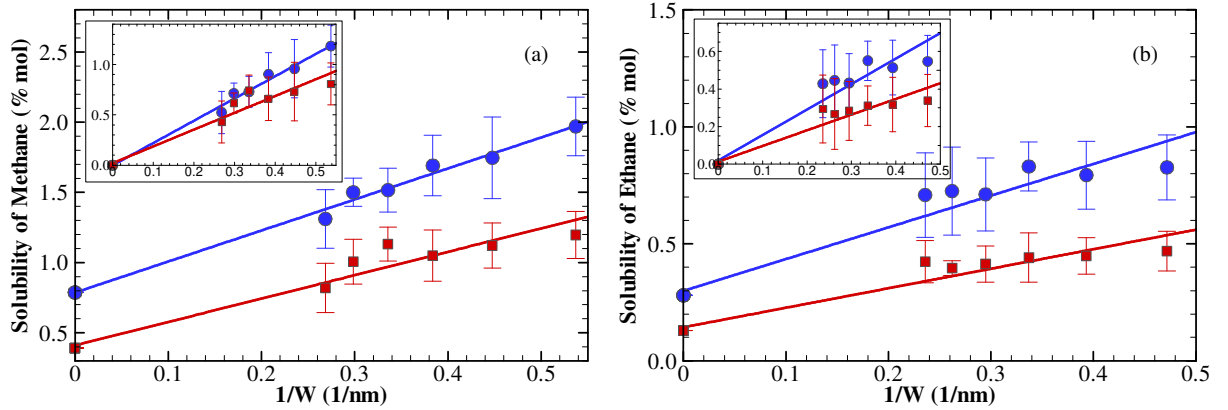


Figure 3: Variation in solubility and over-solubility (inserts) of gas with the inverse of the pore size in the confined region. (a): Methane. (b): Ethane. (Red color) Squares corresponds to $T = 373.15\text{K}$ and $P = 50\text{MPa}$. (Blue color) Circles to $T = 423.15\text{K}$ and $P = 100\text{MPa}$. Solid lines are linear fitting functions.

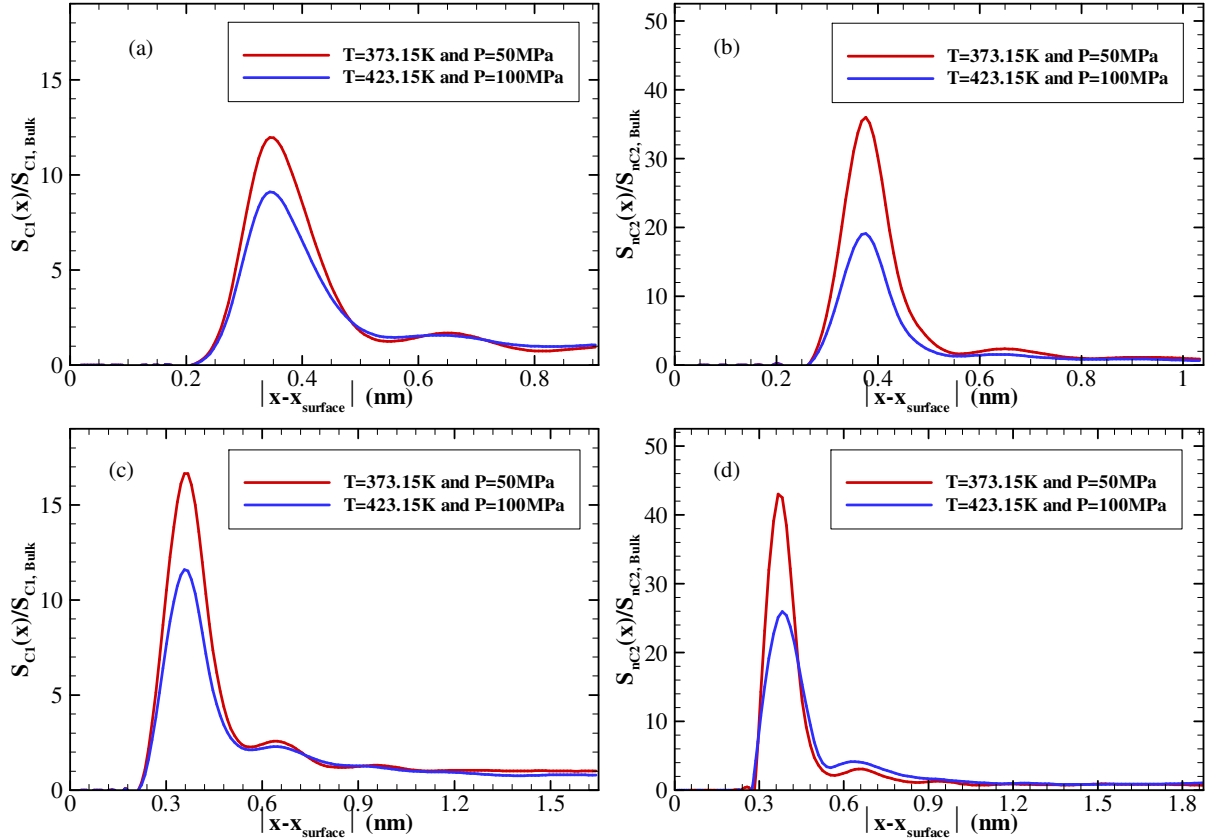


Figure 4: Relative solubility profile of gas in the sampling region (a): Methane in the nanopore of $W=5\sigma_{C1}$. (b): Ethane in the nanopore of $W=5\sigma_{C2}$. (c): Methane in the nanopore of $W=9\sigma_{C1}$. (d): Ethane in the nanopore of $W=9\sigma_{C2}$.

3.2.2. Ethane

The solubility of ethane in the saturated nanopores for the two studied reservoir conditions and for pore sizes ranging from about 2.12 nm to 4.24 nm is displayed in Fig. 3. Results clearly show that the trends for ethane are similar to those found for methane, keeping in mind that ethane is roughly three times less soluble than methane in bulk water.

More precisely, ethane exhibits a local solubility profile similar to that found for methane for both conditions. However, the local increase of solubility close to the solid walls is more pronounced than in methane, reaching up values 40 times larger than the bulk value. Another interesting feature is that the oversolubility of ethane scales well with the inverse of the pore size even if, for the smallest pores, the oversolubility is nearly constant. This behavior is consistent with the adsorption-driven effect combined with a non-negligible contribution related to the confinement-driven effect for the smallest pores, as confirmed by the density profiles shown in Fig. 5.

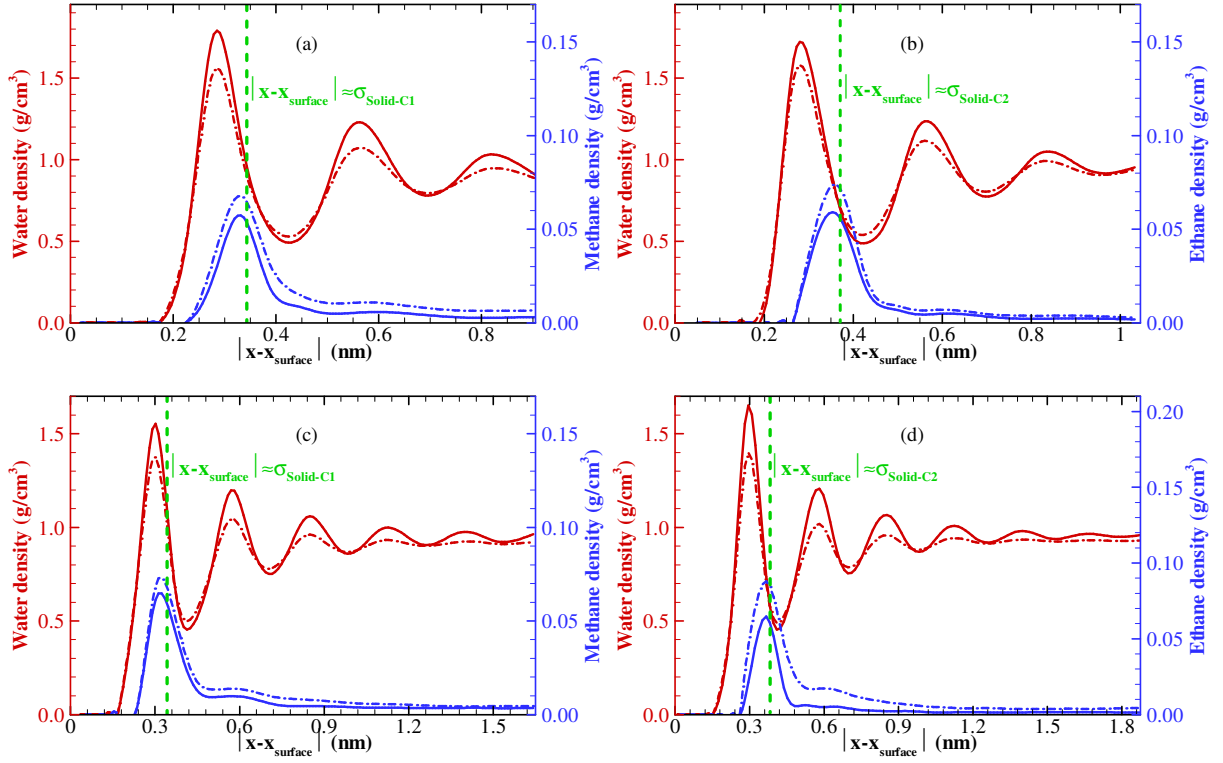


Figure 5: Density profiles of gas and water in the sampling region (a): Methane in the nanopore of $W=5\sigma_{C1}$. (b): Ethane in the nanopore of $W=5\sigma_{C2}$. (c): Methane in the nanopore of $W=9\sigma_{C1}$. (d): Ethane in the nanopore of $W=9\sigma_{C2}$. Solid lines correspond to $T = 373.15\text{K}$ and $P = 50\text{MPa}$ and Dashed-dotted lines correspond to $T = 423.15\text{K}$ and $P = 100\text{MPa}$. (Green color) Vertical dashed lines correspond to a distance of one gas molecular size from the solid surface.

3.3. Effect of the pore size on molecular diffusion

There exist many different formalisms to describe mass diffusion leading to different diffusion coefficients definitions (Cussler, 1997; Wesselingh and Krishna, 2006). This is even more complex in nanopores, even at the pore scale, as the transport coefficients may become space dependent, non-local and non-isotropic (Botan et al., 2011; Hoang and Galliero, 2012b). To keep the problem simple, a 1D Fickian formalism has been chosen to describe the gas diffusion through the saturated nanopores. Such a formalism simply connects the mass flux of the gas to its compositional gradient. A corresponding diffusion coefficient, i.e. Fickian diffusion coefficient D_{Gas} sometimes called transport diffusivity, has been estimated by using a transient non-equilibrium MD (T-NEMD) approach that is rather straightforward to implement in MD simulations (Maginn et al., 1993; Arya et al., 2001), see Fig. 1. This method consists in setting up an initial gas concentration gradient in the simulation system,

and then to monitor the relaxation of the system to the equilibrium state assuming a purely diffusive behavior, as described in section 2.2.

More precisely, to estimate D_{Gas} , the evolution of the molar fraction of the gas in the sampling region $C_{\text{Gas}}(t)$ (averaged over 100 time-steps) has been fitted by a simple 1D diffusion equation as (Witherspoon and Saraf, 1965; Cussler, 1997):

$$\frac{C_{\text{Gas}}(t)}{C_{\text{Gas}}^{\infty}} = 1 - \frac{8}{\pi^2} \sum_n \frac{1}{(2n+1)^2} \exp\left(-[2n+1]^2 \frac{t}{[L^2/\pi^2 D_{\text{Gas}}]}\right) \quad (4)$$

where, C_{Gas}^{∞} is the molar fraction value at equilibrium and L is the characteristic length of the pore over which diffusion occur. The latter has been taken equal to half of the pore length in the y direction plus one molecular diameter of gas to take into account a finite size effect due to the initial configuration setup.

As confirmed by the simulation results shown in Fig. 6, the evolution over time of C_{Gas} can be well fitted by Eq. (4) for both gases, indicating that the T-NEMD approach allows to obtain a good estimation of D_{Gas} , with an uncertainty of about 25%.

3.3.1. Methane

Figure 7 provides the variation in the transport diffusivity of methane relatively to the pore size. Results indicate that the pore size has a slight, but non-negligible, effect on the transport diffusivity. More precisely, D_{C1} tends to decrease with the decrease of the pore size, but this decrease is not very pronounced. This result is consistent with what has been found by many authors on similar systems (Hoang et al., 2010; Hoang and Galliero, 2012a; Zaragoza et al., 2019; Tran et al., 2020; Zhang et al., 2020), which is that the local molecular diffusion of a confined fluid in the plane parallel to the solid surface does not vary significantly with the pore width when dealing with not too strong fluid-solid interaction.

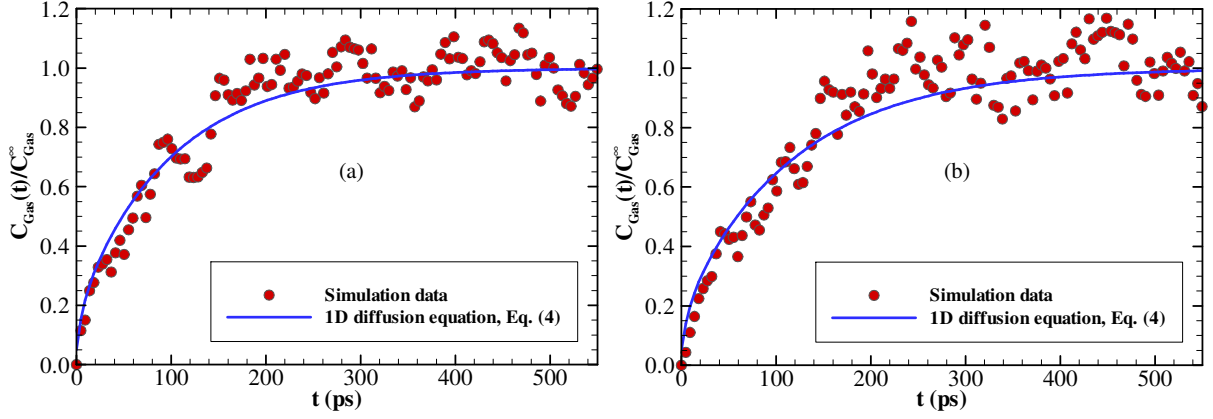


Figure 6: Evolutions of $(C_{\text{Gas}}(t)/C_{\text{Gas}}^{\infty})$ in the sampling region for a pore size equal to 9 times the corresponding gas diameters at the reservoir thermodynamic condition $T = 423.15\text{K}$ and $P = 100\text{MPa}$. (a): Methane. (b): Ethane.

Furthermore, the transport diffusivity of methane in the water-saturated nanopores has been compared with the self-diffusion coefficient of methane in bulk water which is assumed here to be equivalent to the Fickian diffusion coefficient due to the low solubility of gases in water. This diffusion coefficient was computed by performing equilibrium molecular dynamics (EMD) simulations in combination with the usual Einstein's relation (Allen and Tildesley, 1987; Smit and Frenkel, 2002):

$$D_S = \lim_{t \rightarrow \infty} \frac{1}{6t} \langle [\mathbf{r}_i(t) - \mathbf{r}_i(0)]^2 \rangle \quad (5)$$

where, D_S is the self-diffusion coefficient, t is the time, $\langle \dots \rangle$ is the average over molecules and $\mathbf{r}_i(t)$ is the position of molecule i at the time t .

As expected, results indicate that the transport diffusivity of methane is smaller in the confined water than in the bulk water, an effect which is more pronounced at the highest temperature, see Fig. 7. Furthermore, D_{C1} tends to its bulk value for the largest pores. However, the relative effect for the two thermodynamic states is somewhat unexpected as it seems to be more important at $T=423\text{ K}$ and $P=100\text{ MPa}$ which corresponds to a less structured confined water, see Fig. 5.

It is worth noticing that the transport diffusivity of methane obtained here ranges from 4.5×10^{-9} to $10.0 \times 10^{-9} \text{ m}^2/\text{s}$, which is typically one order of magnitude higher than the reported experiment results in porous medium (Schlömer and Krooss, 1997; Schloemer and Krooss, 2004). However, here D_{C1} has been estimated at the pore scale, whereas the transport diffusivity was experimentally deduced at the porous medium scale, i.e. including the effect of tortuosity and porosity (Krooss et al., 1992a; 1992b; Krooss and Leythaeuser, 1997; Song and Zhang, 2013).

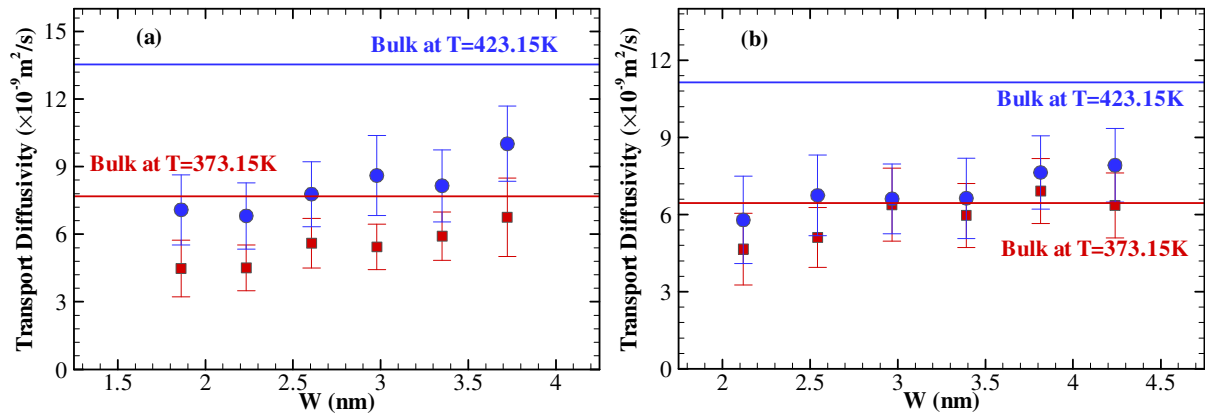


Figure 7: Dependence of transport diffusivity of hydrocarbon gas with the pore size. (a): Methane. (b): Ethane. Squares correspond to the thermodynamic condition $T = 373.15\text{K}$ and $P = 50\text{MPa}$. Circles correspond to $T = 423.15\text{K}$ and $P = 100\text{MPa}$. Lines correspond to the self-diffusion coefficients of gases in bulk water.

3.3.2. Ethane

Pore-size dependence of the transport diffusivity of ethane in the saturated nanopores is shown in Fig. 7. Results indicate that its dependence on pore size is similar to that for methane, showing a slight decrease when the pore size decreases and values tending to the bulk data for the largest pores. In addition, as expected, D_{C2} is slightly smaller than D_{C1} in particular at the highest temperature. The only unexpected result is that the effect of the confinement seems less pronounced, in relative, on ethane than on methane, whereas the ethane molecule is bigger than the methane molecule. This is probably related to the localization of the gases relatively to water in the nanopore. More precisely, the ethane molecules are preferably located around the depleted water region, whereas methane molecules are mostly located in the adsorbed water region, see Fig. 5.

3.4. Leakage of gases through silicate caprock

In the most favorable case from the caprock sealing point of view, the leakage from a gas reservoir is only due to molecular diffusion across the low permeability barrier formed by the caprock. This contribution is often assumed to be negligible in most cases (Schloemer and Krooss, 2004), even if it could play a role in some specific cases (Wang et al., 2018). Thus, it is interesting to revisit the quantification of diffusive gas reservoir leakage over geological times using the previous results obtained on solubility and diffusion of gases in nanopores.

To do so, it has been assumed that the leakage through the caprock is simply governed by a 1D diffusion process. In this framework, the cumulative amount of gas leakage per unit of caprock surface over a time t can be estimated from (Krooss et al., 1992a; 1992b; Schlömer and Krooss, 1997):

$$Q_{\text{Gas}}(t) = \left(\frac{D_{\text{Gas}}^{\text{Eff}} C_{\text{Gas}} \phi}{L_{\text{Cap}}} t + \frac{2C_{\text{Gas}} \phi L_{\text{Cap}}}{\pi^2} \sum_{n=1} \frac{1}{n^2} \left[1 - \exp\left(-\frac{n^2 D_{\text{Gas}}^{\text{Eff}} \pi^2}{L_{\text{Cap}}^2} t\right) \right] \right) \quad (6)$$

where, ϕ is the porosity, L_{Cap} is the thickness of the caprock, and $D_{\text{Gas}}^{\text{Eff}}$ is the effective transport diffusivity that is defined as D_{Gas}/ζ with ζ being the tortuosity (Song and Zhang, 2013). As an example, the model caprock considered in this work is assumed to possess a thickness of 100m, a porosity of 1% and a tortuosity of 50, and is composed of water-saturated nanopores having a pore size distribution peaked on 3nm (Schlömer and Krooss, 1997; Kampman et al., 2016; Espinoza and Santamarina, 2017).

Evolutions of cumulative amount of gases leakage through the model caprock are shown in Fig. 8. They have been computed from the 1D diffusion process Eq. (6) using the solubility and the transport diffusivity values of gases in the saturated nanopore and in the bulk water over 50 millions of years. Interestingly, results clearly indicate that the nano-confinement effects are able to noticeably increase the leakage of gases compared to what would be deduced without them.

The increased leakage compared to what could be estimated without taking into account the effects of nano-confinement reflects the fact that the oversolubility is dominant over the decrease of diffusion coefficient. More precisely, on geological time, this leakage increase can be approximated, see Eq. (6), by the ratio of the product $D_{\text{Gas}}^{\text{Eff}} C_{\text{Gas}}$ under confinement relatively to its value in bulk water. From our data this means an increase in gas leakage of about 165% for methane and 265% for ethane. Even if evaluated on an oversimplified system, this result indicates that the estimation of the diffusive leakage of gases through caprock should take into account the influence of nano-confinement effects.

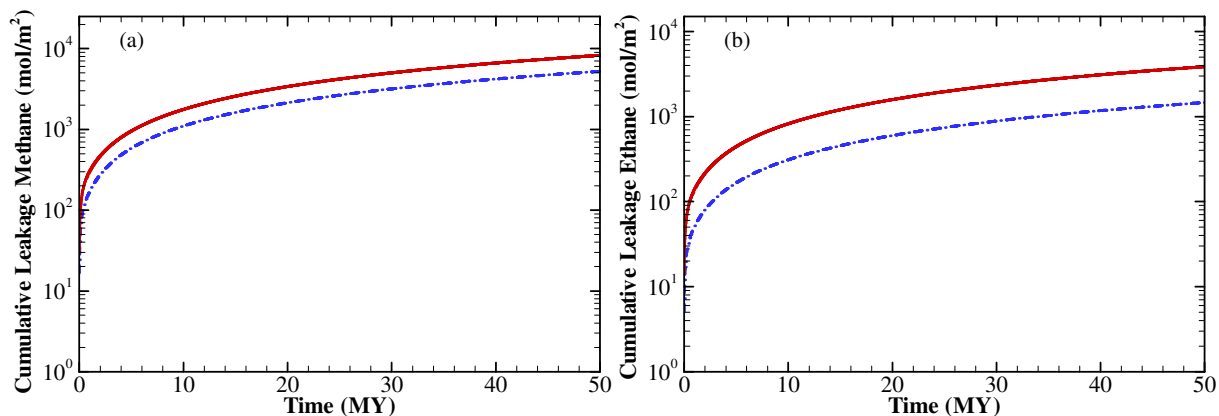


Figure 8: Cumulative amount of hydrocarbon gases leaking through the caprock by the molecular diffusion at the reservoir thermodynamic condition $T = 373.15\text{K}$ and $P = 50\text{MPa}$. (a) Methane. (b) Ethane. (Red color) Solid lines correspond to D_{Gas} and C_{Gas} of gases in the saturated nanopores (with taking into account the effect of confinement). (Blue color) Dashed-Dotted lines correspond to D_{Gas} and C_{Gas} of gases in bulk water (without taking into account the effects of confinement).

4. Conclusions

In this work, molecular dynamics simulations have been performed in grand canonical like ensemble to investigate the solubility and transport diffusivity of light hydrocarbon gases (methane and ethane) in water-saturated slit nanopores at reservoir thermodynamics conditions, ($T=373.15\text{K}$, $P=50\text{MPa}$) and ($T=423.15\text{K}$, $P=100\text{MPa}$). For simplicity, all fluid and solid molecules have been modelled by Lennard-Jones (LJ) particles. Fluid LJ parameters have been adjusted to yield a set of target properties, such as density, viscosity and solubility, in good agreement with the experiments. Solid parameters, including the LJ potential and structure, have been chosen to quantitatively represent the roughness and surface energy characteristics of silicate mineral surfaces.

Very interestingly, it has been shown that the solubility of hydrocarbon gases in the water-saturated nanopores is significantly higher than that in bulk water (so-called oversolubility). This results from the local gas solubility which is strongly enhanced in the vicinity of the solid surface and can be up to 15 times (40 times) higher than the solubility of methane (ethane) in bulk water. Such a behavior is mainly induced by an adsorption-driven effect for methane, whereas there is an additional non-negligible contribution due to a confinement-driven effect for ethane. As a consequence, it has been shown that the oversolubility linearly increases with the reciprocal of the pore size.

Regarding the transport diffusivity of hydrocarbon gases in the water-saturated nanopores which has been estimated by using a “transient” non-equilibrium molecular dynamic (T-NEMD) approach, it has been shown that the pore size has a weak, but non-negligible impact on it. More precisely, the transport diffusivity decreases with the decrease of the pore size. However, this effect is more pronounced on methane than on ethane which is rather surprising as methane molecules are smaller than ethane molecules. This is probably due to the fact that methane is mostly located at the adsorbed water region in the nanopore, whereas ethane is mainly located in the depleted water region.

Finally, these results have been used to quantify the diffusive gas leakage through an idealized water-saturated caprock over geological time thanks to a 1D diffusion model. Results have shown that the nano-confinement effects can noticeably enhance the leakage of gases by diffusion, because the effect of oversolubility of gases under confinement is dominant over the decrease of diffusivity transport due to pore size. This result, even if deduced from an oversimplified system compared to real cases, emphasizes the importance of taking into account nano-confinement effects on gas leakage estimates.

Acknowledgements

We gratefully acknowledge TOTAL S.A. for the post-doctoral grant awarded to two of us (BKB and HH) and for letting us publish these results. We also thank the Pau University and the MCIA for providing computational facilities.

References

- Allen, M.P., Tildesley, D.J., 1987. *Computer Simulations of Liquids*. Oxford University Press, New York.
- Arya, G., Chang, H.C., Maginn, E.J., 2001. A critical comparison of equilibrium, non-equilibrium and boundary-driven molecular dynamics techniques for studying transport in microporous materials. *J. Chem. Phys.* **115**, 8112-8124.
- Baghooee, H., Montel, F., Galliero, G., Yan, W., Shapiro, A., 2021. A new approach to thermal segregation in petroleum reservoirs: Algorithm and case studies, *J. Pet. Sci. Eng.* **201**, 108367.
- Berendsen, H.J.C., Postma, J.P.M., van Gunsteren, W.F., Di Nola, A., Haak, J.R., 1984. Molecular dynamics with coupling to an external bath. *J. Chem. Phys.* **81**, 3684.
- Botan, A., Roenberg, B., Marry, V., Turq, P., Noetinger, B., 2011. Hydrodynamics in Clay Nanopores. *J. Phys. Chem. C* **115**, 16109-16115.
- Bui, T., Phan, A., Cole, D.R., Striolo, A., 2017. Transport mechanism of guest methane in water-filled nanopores. *J. Phys. Chem. C* **121**, 15675-15686.
- Campos, M.D., Akkutlu, I.Y., Sigal, R.F., 2009. A molecular dynamics study on natural gas solubility enhancement in water confined to small pores. SPE-124491-MS.
- Cussler, E.L., 1997. *Diffusion - Mass Transfer in Fluid Systems*, 2nd Edition, Cambridge University Press.
- Dembicki, H., 2016. *Practical Petroleum Geochemistry for Exploration and Production*. Elsevier.
- Duan, Z., Mao, S., 2006. A thermodynamic model for calculating methane solubility, density and gas phase composition of methane-bearing aqueous fluids from 273 to 523 K and from 1 to 2000 bar, *Geochim. Cosmochim. Acta.* **70**, 3369-3386.
- Espinoza, D.N., Santamarina, J.C., 2017. CO₂ breakthrough - Caprock sealing efficiency and integrity for carbon geological storage. *Int. J. Greenh. Gas Con.* **66**, 218-229.
- Gadikota, G., Dazas, B., Rother, G., Cheshire, M.C., Bourg, I.C., 2017. Hydrophobic solvation of gases (CO₂, CH₄, H₂, noble gases) in clay interlayer nanopores, *J. Phys. Chem. C* **121**, 26539-26550.
- Galliero, G., Boned, C., Baylaucq, A., 2005. Molecular Dynamics Study of the Lennard-Jones Fluid Viscosity: Application to Real Fluids. *Ind. Eng. Chem. Res.* **44**, 6963-6972.
- Galliero, G., Boned, C., Baylaucq, A., Montel, F., 2006. Molecular dynamics comparative study of Lennard-Jones -6 and exponential -6 potentials: Application to real simple fluids (viscosity and pressure). *Phys. Rev. E* **73**, 061201.

Grekov, D., Suzuki-Muresan, T., Kalinichev, A.G., Pré, P., Grambow, B., 2020. Thermodynamic data of adsorption reveal the entry of CH₄ and CO₂ in smectite clay interlayer. *Phys. Chem. Chem. Phys.* **22**, 16727-16733.

Grunau, H.R., 1987. A worldwide look at the cap-rock problem. *J. Pet. Geol.* **10**, 245-266.

Hadley, K., McCabe, C., 2012. Coarse-Grained Molecular Models of Water: A review. *Mol. Simul.* **38**, 671-681.

Hamani, A.W.S., Hoang, H., Viet, T.Q.Q., Daridon, J.L., Galliero, G., 2020. Excess volume, isothermal compressibility, isentropic compressibility and speed of sound of carbon dioxide+n-heptane binary mixture under pressure up to 70 MPa. II. Molecular simulations. *J. Supercrit. Fluids.* **164**, 104890.

Ho, L.N., Clauzier, S., Schuurman, Y., Farrusseng, D., Coasne, B., 2013. Gas uptake in solvents confined in mesopores: Adsorption versus enhanced solubility. *J. Phys. Chem. Lett.* **4**, 2274-2278.

Ho, L.N., Schuurman, Y., Farrusseng, D., Coasne, B., 2015. Solubility of gases in water confined in nanoporous materials: ZSM-5, MCM-41, and MIL-100. *J. Phys. Chem. C* **119**, 21547-21554.

Hoang, H., Kang, S., Suh, K., 2010. Molecular dynamics study on the effect of solution-wall interaction potential on the properties of solution in uniformly charged hydrophobic channel, *J. Mech. Sci. Tech.*, **24**, 1401-1410.

Hoang, H., Galliero, G., 2012a. Grand canonical-like molecular dynamics simulations: Application to anisotropic mass diffusion in a nanoporous medium, *J. Chem. Phys.* **136**, 184702.

Hoang, H., Galliero, G., 2012b. Local viscosity of a fluid confined in a narrow pore. *Phys. Rev. E* **86**, 021202.

Hoang, H., Galliero, G., 2013. Shear behavior of a confined thin film: Influence of the molecular dynamics scheme employed. *J. Chem. Phys.* **138**, 054707.

Hoang, H., Delage-Santacreu, S., Galliero, G., 2017. Simultaneous Description of Equilibrium, Interfacial, and Transport Properties of Fluids Using a Mie Chain Coarse-Grained Force Field. *Ind. Eng. Chem. Res.*, **56**, 9213-9226.

Hoang, H., Nguyen, P., Pujol, M., Galliero, G., 2019. Elemental and isotopic fractionation of noble gases in gas and oil under reservoir conditions: Impact of thermodiffusion. *Eur. Phys. J. E* **42**, 61.

Hoang, H., Ho, K. H., Battani, A., Pujol, M., Galliero, G., 2021. On Elemental and Isotopic Fractionation of Noble Gases in Geological Fluids by Molecular Diffusion. *Geochim. Cosmochim. Acta*, *In Press*.

Israelachvili, J., 2010. Intermolecular and Surface Forces. Third ed., Academic, Amsterdam.

Iwamatsu, M., 1998. A molecular theory of solvation force oscillations in nonpolar liquids. *J. Colloid Interface Sci.* **204**, 374-388.

Kampman, N., Busch, A., Bertier, P., Snippe, J., Hangx, S., Pipich, V., Di, Z., Rother, G., Harrington, J.F., Evans, J.P., Maskell, A., Chapman, H.J., Maskell, M.J., 2016. Observational evidence confirms modelling of the long-term integrity of CO₂-reservoir caprocks. *Nat. Commun.* **7**, 1-10.

Karniadakis, G., Beskok, A., Aluru, N., 2004. *Microflows and Nanoflows*. Springer Science + Business Media, New York.

Kolafa, J., Nezbeda, I., 1994. The Lennard-Jones fluid: an accurate analytic and theoretically-based equation of state. *Fluid Phase Equilib.* **100**, 1-34.

Krooss, B.M., Leythaeuser, D., Schaefer, R.G., 1988. Light hydrocarbon diffusion in a caprock. *Chem. Geol.* **71**, 65-76.

Krooss, B.M., Leythaeuser, D., Schaefer, R.G., 1992a. The quantification of diffusive hydrocarbon losses through cap rocks of natural gas reservoirs - A reevaluation, *Am. Assoc. Petrol. Geol. Bull.* **76**, 403-406.

Krooss, B.M., Leythaeuser, D., Schaefer, R.G., 1992b. The quantification of diffusive hydrocarbon losses through cap rocks of natural gas reservoirs - A reevaluation: Reply. *Am. Assoc. Petrol. Geol. Bull.* **76**, 1842-1846.

Krooss, B.M., 1992. Diffusive losses of hydrocarbons through cap rock. Experimental studies and theoretical considerations. *Erdol and Kohle - Erdgas - Petrochemie/ Hydrocarbon Technology* **45**, 387-396.

Krooss, B.M., Leythaeuser, D., 1997. Diffusion of methane and ethane through the reservoir cap rock; implications for the timing and duration of catagenesis: Discussion. *Assoc. Petrol. Geol. Bull.* **81**, 155-161.

Lemmon, E.W.; Huber, M.L.; McLinden, M.O., 2007. Reference Fluid Thermodynamic and Transport Properties, NIST Standard Reference Database 23; REFPROP Version 8.0.

Lennard-Jones, J.E., 1937. The electronic structure of some polyenes and aromatic molecules I-The nature of the links by the method of molecular orbitals. *Proc. R. Soc. Lond. Ser. A Math. Phys. Eng. Sci.* **158**, 280-296.

- Li, J., Li, X., Wang, X., Li, Y., Wu, K., Shi, J., Yang, L., Feng, D., Zhang, T., Yu, P., 2016. Water distribution characteristic and effect on methane adsorption capacity in shale clay. *Inter. J. Coal Geol.* **159**, 135-154.
- Liu, C.C., Chou, H.J., Lin, C.Y., Janmanchi, D., Chung, P.W., Mou, C.Y., Yu, S.S.F., Chan, S.I., 2020. The oversolubility of methane gas in nano-confined water in nanoporous silica materials. *Micropor. Mesopor. Mat.* **293**, 109793.
- Maginn, E.J., Bell, A.T., Theodorou, D.N., 1993. Transport Diffusivity of Methane in Silicalite from Equilibrium and Nonequilibrium Simulations. *J. Phys. Chem.* **97**, 4173-4181.
- Mao, S., Zhang, Z., Hu, J., Sun, R., Duan, Z., 2005. An accurate model for calculating C₂H₆ solubility in pure water and aqueous NaCl solutions, *Fluid Phase Equilib.* **238**, 77-86.
- Martin, M.G., Siepmann, J.I., 1998. Transferable potentials for phase equilibria. 1. United atom description of n-alkanes, *J. Phys. Chem. B* **102**, 2569-2577.
- Miachon, S., Syakaev, V.V., Rakhmatullin, A., Pera-Titus, M., Caldarelli, S., Dalmon, J.A., 2008. Higher gas solubility in nanoliquids?. *ChemPhysChem.* **9**, 78-82.
- Montel, F., Bickert, J., Lagisquet, A., Galliero, G., 2007. Initial state of petroleum reservoirs: A comprehensive approach, *J. Pet. Sci. Eng.* **58**, 391-402.
- Müller, E.A., Gelb, L.D., 2003. Molecular modeling of fluid-phase equilibria using an isotropic multipolar potential, *Ind. Eng. Chem. Res.* **42**, 4123-4131.
- Nowamooz, A., Lemieux, J.M., Molson, J., Therrien, R., 2015. Numerical investigation of methane and formation fluid leakage along the casing of a decommissioned shale gas well. *Water Resour. Res.* **51**, 4592-4622.
- Phan, A., Cole, D.R., Striolo, A., 2014. Aqueous methane in slit-shaped silica nanopores: high solubility and traces of hydrates. *J. Phys. Chem. C* **118**, 4860-4868.
- Phan, A., Cole, D.R., Weiß, R.G., Dzubiella, J., Striolo, A., 2016. Confined water determines transport properties of guest molecules in narrow pores. *ACS Nano.* **10**, 7646-7656.
- Schloemer, S., Krooss, B. M., 2004. Molecular transport of methane, ethane and nitrogen and the influence of diffusion on the chemical and isotopic composition of natural gas accumulations. *Geofluids*, **4**, 81-108.
- Schlömer, S., Krooss, B.M., 1997. Experimental characterisation of the hydrocarbon sealing efficiency of cap rocks. *Mar. Pet. Geol.* **14**, 565-580.
- Schnabel, T., Vrabec, J., Hasse, H., 2007. Unlike Lennard–Jones parameters for vapor-liquid equilibria. *J. Mol. Liq.* **135**, 170-178.
- Selley, R.C., Sonnenberg, S.A., 2015. *Elements of Petroleum Geology*. 3rd Edition, Academic Press.

- Smit, B., Frenkel, D., 2002. *Understanding Molecular Simulation: From Algorithms to Applications*, 2nd Editions, Academic Press.
- Song, J., Zhang, D., 2013. Comprehensive review of caprock-sealing mechanisms for geologic carbon sequestration. *Environ. Sci. Technol.* **47**, 9-22.
- Soreide, I., Whitson, C., 1992. Peng-Ronbinson predictions for hydrocarbons, CO₂, N₂, and H₂S with pure water and NaCl brine. *Fluid Phase Equilib.* **77**, 217-240.
- Sun, R., Duan, Z., 2007. An accurate model to predict the thermodynamic stability of methane hydrate and methane solubility in marine environments. *Chem. Geol.* **244**, 248-262.
- Tran, T.H., Phan, G.T.T., Luc, H.T., Nguyen, P.T., Hoang, H., 2020. Molecular dynamics simulations on aqueous solution confined in charged nanochannels: Asymmetric effect of surface charge. *Mol. Simul.* **46**, 796-804.
- Verlet, L., 1967. Computer "Experiments" on classical fluids. I. Thermodynamical properties of Lennard-Jones molecules. *Phys. Rev.* **159**, 98.
- Wang, Y., Chen, J., Pang, X., Zhang, B., Wang, Y., He, L., Chen, Z., Zhang, G., 2018. Anomalies of natural gas compositions and carbon isotope ratios caused by gas diffusion—A case from the Donghe Sandstone reservoir in the Hadexun Oilfield, Tarim Basin, northwest China. *J. Asian Earth Sci.* **156**, 75-89.
- Wesselingh, J.A., Krishna, R., 2006. *Mass Transfer in Multicomponent Mixtures*, VSSD.
- Witherspoon, P.A., Saraf, D.N., 1965. Diffusion of Methane, Ethane, Propane, and n-Butane in Water from 25 to 43°. *J. Phys. Chem.* **69**, 3752-3755.
- Yuan, W., Pan, Z., Li, X., Yang, Y., Zhao, C., Connell, L.D., Li, S., He, J., 2014. Experimental study and modelling of methane adsorption and diffusion in shale. *Fuel.* **117**, 509-519.
- Zaragoza, A., Gonzalez, M. A., Joly, L., López-Montero, I., Canales, M. A., Benavides, A. L., Valeriani, C., 2019. Molecular dynamics study of nanoconfined TIP4P/2005 water: How confinement and temperature affect diffusion and viscosity. *Phys. Chem. Chem. Phys.* **21**, 13653-13667.
- Zhang, L., Liu, C., Liu, Y., Li, Q., Cheng, Q., Cai, S., 2020. Transport Property of Methane and Ethane in K-Illite Nanopores of Shale: Insights from Molecular Dynamic Simulations. *Energ. Fuel.* **34**, 1710-1719.